JOURNAL OF GEOPHYSICAL RESEARCH, VOL. 106, NO. D16, PAGES 18,113–18,129, AUGUST 27, 2001

A model for prediction of desert dust cycle in the atmosphere

Slobodan Nickovic

Euro-Mediterranean Centre on Insular Coastal Dynamics (ICoD), University of Malta, Foundation for International Studies, Valletta, Malta

George Kallos, Anastasios Papadopoulos, and Olga Kakaliagou

University of Athens, Department of Applied Physics, Athens, Greece

Abstract. An integrated modeling system has been developed to accurately describe the dust cycle in the atmosphere. It is based on the SKIRON/Eta modeling system and the Eta/NCEP regional atmospheric model. The dust modules of the entire system incorporate the state of the art parameterizations of all the major phases of the atmospheric dust life such as production, diffusion, advection, and removal. These modules also include effects of the particle size distribution on aerosol dispersion. The dust production mechanism is based on the viscous/turbulent mixing, shear-free convection diffusion, and soil moisture. In addition to these sophisticated mechanisms, very high resolution databases, including elevation, soil properties, and vegetation cover are utilized. The entire system is easily configurable and transferable to any place on the Earth, it can cover domains on almost any size, and its horizontal resolution can vary from about 100 km up to approximately 4 km. It can run on one-way-nested form if necessary. The performance of the system has been tested for various dust storm episodes, in various places and resolution using gridded analysis or forecasting fields from various sources (ECMWF and NCEP) for initial and boundary conditions. The system is in operational use during the last two years, providing 72 hour forecasts for the Mediterranean region. The results are available on the internet (http://www.icod.org.mt and http://forecast.uoa.gr).

1. Introduction

A large amount of mineral dust is mobilized over arid regions and injected into the atmosphere under favorable weather conditions. Estimates of global dust input based on ground measurements, satellite sensing, and modeling studies range from several hundreds to several thousands megatons per year [*Dulac et al.*, 1992; *Tegen and Fung*, 1994]. As observations indicate, there is a large seasonal variability of the dust cycle that is strongly correlated with the global atmospheric circulation [*Moulin et al.*, 1997].

Although mineral dust has not been usually considered as a significant global climate-forcing factor, recent studies [*Tegen and Fung*, 1994; *Li et al.*, 1996] substantially change the picture about this subject. In contrast to the greenhouse gases, which affect only the long-wave radiation, dust particles modify both short- and long-wave radiation components [*Andreae*, 1996]. In the visible part of the energy spectrum, dust aerosol scatters back to space part of the solar energy, thus generating net cooling rates that are of the same order of magnitude as heating by the greenhouse gases. In the infrared part, dust acts as an absorber and therefore warms the Earth.

Another important effect of the dust cycle is the triggering of various biochemical reactions between dust ingredients and the environment. After depositing over the ocean surface, desert dust containing active iron and phosphorus can cause algal blooms over the surface ocean water [e.g., *Dulac et al.*, 1996]. In such processes, dust modifies biochemistry of the ocean water [*Martin and Fitzwater*, 1988; *Kremling and Streau*, 1993], changes features of the terrestrial ecosystems [*Reichholf*, 1986], and neutralizes acid rains [*Hedin and Likens*, 1996]

In regions with high soil erosion, dust behaves as a pollutant that significantly reduces the air quality. In these areas, ambient dust concentration during dust storms may significantly exceed international standards for allowable concentrations [*Nickling and Gillies*, 1993] and therefore cause health problems such as allergy, respiratory diseases, and eye infections. Recently, cases of life loose and property damages during extreme dust storm events were recorded in Sudan (May 1996) and Egypt (May 1997).

Substantial impacts of dust on climate and environment have increased needs to better understand and, eventually, predict the atmospheric dust cycle. Following such interest, several numerical dust models have been developed [*Westphal et al.*, 1987, 1988; *Joussaume*, 1990; *Tegen and Fung*, 1994; *Nickovic and Dobricic*, 1996; *Nickovic et al.*, 1997a] and used for studying dust process.

In this article we describe in detail a dust modeling system: the Dust REgional Atmospheric Modeling (DREAM) system. DREAM is based on the initial work of *Nickovic and Dobricic* [1996]. It is divided in two main parts: (1) the atmospheric modeling system and (2) the dust concentration module

The atmospheric modeling system used for the development is the SKIRON forecasting system [*Kallos et al.*, 1997; *Nickovic et al.*, 1997], which is based on the 1997 version of the Eta/NCEP (National Centers for Environmental Prediction). Compared to the Eta model used in our previous dust experiments [*Nickovic and Dobricic*, 1996], the actual

Paper number 2000JD900794.
0148-0227/01/2000JD900794$09.00

model version contains several new improvements: a new positive-definite shape-preserving advection scheme (also applied to dust concentration field), the turbulent mixing scheme, and new schemes for the atmospheric radiation and surface land processes.

The second module introduces a number of new improvements compared to solutions we used by *Nickovic and Dobricic* [1996]. First, a new scheme for dust production is applied on the basis of a more sophisticated parameterization of dust mobilization process. Second, a four-particle instead of the previous one-particle size scheme is implemented in order to simulate more accurately the size-dependent processes. Third, the topography, soil, and vegetation-type data used are of higher resolution than the original Eta/NCEP model utilizes. This is absolutely necessary in order to provide more appropriate surface boundary conditions for both the atmospheric and the dust modules. Finally, a new parameterization scheme for dry deposition is applied.

The mutual aerosol-atmosphere interaction is not included in the current model, assuming that dust-radiation effects do not considerably influence atmospheric processes of timescales covered in our model tests. However, this task will be a subject of future development.

2. Modeling Aspects

A major development of the initial model of *Nickovic and Dobricic* [1996] was developed at the framework of MEDUSE (funded by DG-XII of the European Union) and SKIRON (funded by the European Union and General Secretariat of Science and Technology of Greece) projects. The entire system was used operationally during the MEDUSE project during the period March 1997 to April 1998. The system predicted most of the major dust transport events in the Mediterranean. In addition, different versions of the system were used to perform studies of historical dust-storm events [*Nickovic et al*, 1997a, 1997b; *Krichak et al.*, 1999; *Kubilay et al.*, 2000]. Further development of the DREAM system was performed during the following years, up to now.

The dynamics of the Eta/NCEP model (October 1997 version) is based on large-scale numerical solutions controlled by conservation of integral properties [*Arakawa*, 1966; *Janjic*, 1977, 1984], energetically consistent time-difference splitting [*Janjic*, 1979, 1997], and the step-like mountain representation [*Mesinger et al.*, 1988]. For horizontal advection of passive substances (including dust concentration), a conservative positive definite scheme [*Janjic*, 1997] has been applied. The model physics consists of the viscous sublayer models over water [*Janjic*, 1994] and over land [*Zilitinkevitch*, 1995], the surface layer scheme based on the similarity theory [*Janjic*, 1996b], a turbulence closure scheme based on Kolmogorov-Heisenberg theory [*Janjic*, 1996a], the Betts-Miller-Janjic deep and shallow moist convection scheme [*Betts*, 1986; *Janjic*, 1994], the land surface scheme [*Chen et al.*, 1996], the grid-scale precipitation scheme [*Zhao and Carr*, 1997], and the radiation scheme [*Lacis and Hansen*, 1974; *Fels and Schwartzkopf*, 1975].

In DREAM the desert dust cycle is described by a set of K-independent Euler-type concentration equations:

$$\frac{\partial C_k}{\partial t} = -u\frac{\partial C_k}{\partial x} - v\frac{\partial C_k}{\partial y} - \left(w - v_{gk}\right)\frac{\partial C_k}{\partial z} - \nabla\left(K_H \nabla C_k\right) - \frac{\partial}{\partial z}\left(K_Z \frac{\partial C_k}{\partial z}\right) + \left(\frac{\partial C_k}{\partial t}\right)_{\text{SOURCE}} - \left(\frac{\partial C_k}{\partial t}\right)_{\text{SINK}},$$

$$k=1,\ldots K \qquad (1)$$

allowing no interparticle interactions. Here K indicates the number of particle size classes. Following *Tegen and Fung* [1994], we consider that there are K=4 particle size classes determined by clay, small silt, large silt, and sand. C_k is the dust concentration of a kth particle size class, u and v are the horizontal velocity components, w is the vertical velocity, v_{gk} is the gravitational settling velocity, ∇ is the horizontal nabla operator, K_H is the lateral diffusion coefficient, K_Z is the turbulence exchange coefficient, $(\partial C_k/\partial t)_{\text{SOURCE}}$ is the source, and $(\partial C_k/\partial t)_{\text{SINK}}$ is the sink term, which includes both wet and dry deposition fractions.

The total concentration C is a weighted sum of concentrations of K particle size classes:

$$C = \sum_{k=1}^{K} \delta_k C_k; \qquad \sum_{k=1}^{K} \delta_k = 1. \qquad (2)$$

Here δ_k denotes a mass fraction of the kth particle category, which will be specified later on.

2.1. Dust Sources

Wind erosion of the soil is controlled mainly by the following factors: (1) type of soil, (2) type of vegetation cover, (3) soil moisture content, and (4) surface atmospheric turbulence.

The injected dust concentration rates are calculated through the following steps:

2.1.1. Step 1. Grid points acting as desert dust sources in the model are specified using arid and semiarid categories of the global vegetation data set. This is done by mapping the global vegetation data into the horizontal model grid and by counting numbers of desert points falling into Eta/NCEP model grid boxes The fraction of a grid point area covered by desert surface is calculated by

$$a = \frac{\text{number of dust points in model grid box}}{\text{total number of vegetation points in model grid box}}. \qquad (3)$$

2.1.2. Step 2. The global soil texture types are mapped into the horizontal model grid. For each texture class the β fractions of clay, small silt, large silt, and sand are estimated.

2.1.3. Step 3. The typical particle size radii and particle densities for the four classes considered of clay, small silt, large silt, and sand are defined. The ratio γ of the mass available for uplift and the total mass of the respective size class [*Tegen and Fung*, 1994] is estimated.

2.1.4. Step 4. Combining α, β, and γ from the previous steps, the dust productivity factor δ is calculated.

2.1.5. Step 5. The first four steps are done in the preprocessing phase, before the actual model execution begins. During the model run, the prognostic atmospheric and hydrological conditions are used in order to calculate the effective rates of the injected dust concentration.

Table 1. Desert Masks According to Vegetation in the Olson World Ecosystem Data

Code Number	Vegetation Type	Desert Mask M
8	desert, mostly bare stone, clay, and sand	1.0
50	sand desert, partly blowing dunes	1 0
51	semidesert/desert scrub/sparse grass	0.5
52	cool/cold shrub semidesert/steppe	0 5
others	/	0

2.2. Grid Mapping of Vegetation and Soil Texture Type Data

High resolution fields of vegetation and soil/texture types were prepared [*Papadopoulos et al.*, 1997] as input data for the surface process schemes of the atmospheric driving model. At the same time, the same data is used for the specification of dust sources and for the calculation of dust-related processes dependent on soil conditions.

To define the geographical distribution of vegetation, a subjective correspondence is established between the Olson World Ecosystems [*EPA*, 1992] with 59 classes at 10 min resolution, and the thirteen (SSiB) vegetation types [*Wilson and Henderson-Sellers*, 1985] required by the Eta/NCEP model. The data are then mapped into the Eta/NCEP grid. The correspondence between these two vegetation data sets has been proceeded according to the literature [*Corine*, 1993; *Wilson and Henderson-Sellers*, 1985].

The dust productive areas are distinguished from the others by the desert/no-desert mask M calculated from vegetation types given in Table 1.

Depending on $\varepsilon=(\Delta_{ETA}/\Delta_{VEG})$, the ratio between the horizontal grid resolution of the Eta model Δ_{ETA} and the resolution of the global vegetation data set Δ_{VEG}, one of the following methods to calculate the fraction of the model grid box covered by desert surface is applied:

2.2.1. $\varepsilon > 1$. In this case each model grid box contains at least one point from the global vegetation grid, and thus (3) is calculated as

$$\alpha^{i,j} = \frac{\sum_{n=1}^{N} M_n^{i,j}}{N}. \quad (4a)$$

Here i and j are horizontal indices of a model grid box; N is the total number of points from the global data falling into $\alpha(i, j)$ grid box.

2.2.2. $\varepsilon < 1$. In this case some model grid boxes may not contain any point from the global vegetation grid. Here α is the interpolated value of the desert mask M from the four nearest global grid points surrounding a model grid point:

$$\alpha^{i,j} = \sum_{m=1}^{4} \psi_m^{i,j} M_m^{i,j}. \quad (4b)$$

The summation above is done over four nearest global grid points surrounding a model grid point (i,j), and ψ_m is the bilinear interpolation-weighting factor. Figure 1 graphically illustrates two considered methods of calculating $\alpha^{i,j}$.

To specify soil texture classes required by the Eta/NCEP model, two data sets are used [*EPA*, 1992]: (1) the Staub and Rosenzweig Zobler near-surface soil texture (referred to as ZOBLER) at 1° resolution, consisting of seven textural classes, and (2) the UNEP/GRID gridded FAO/UNESCO soil units (referred to as FAO) at 2 min resolution consisting of soil units with 134 legends. To define correspondence between two soil data sets having different resolutions, 2 min 900 FAO values are corresponded to one 1° ZOBLER class

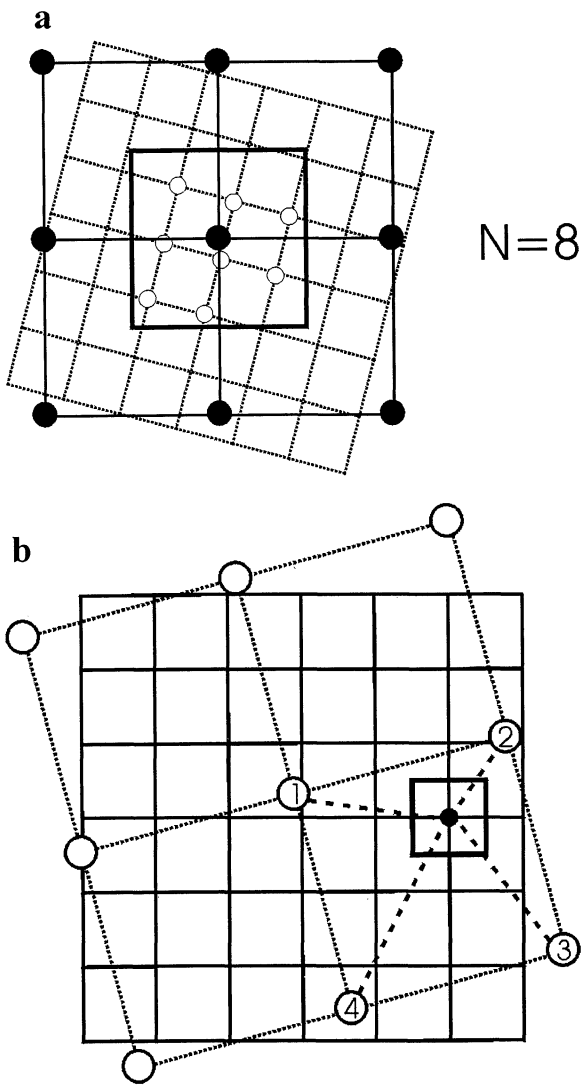

Figure 1. Specification of the model grid fraction covered by desert. The boldface-line and the dashed-line grids carry the vegetation/desert data and the model variables, respectively. (a) Example with N=8 vegetation/desert points inside the model grid box (boldface outline of square); fractions are calculated using equation (4a). (b) Example with no vegetation/desert points inside the model grid box; fractions are calculated using equation (4b)

Table 2. Correspondence Between Texture Classes and Soil Types, and Relative Contributions of Clay/Sand/Silt

l	ZOBLER Texture Classes	Cosby Soil Types	β_{kl} Clay	Small Silt	Large Silt	Sand
1	coarse	loamy sand	0.12	0.08	0.08	0.80
2	medium	silty clay loam	0.34	0.56	0.56	0.10
3	fine	clay	0 45	0.30	0 30	0.25
4	coarse-medium	sandy loam	0.12	0.18	0.18	0.70
5	coarse-fine	sandy clay	0 40	0.10	0 10	0.50
6	medium-fine	clay loam	0.34	0.36	0.36	0 30
7	coarse-medium-fine	sandy clay loam	0.22	0.18	0.18	0.60

inside each ZOBLER grid box. By selecting one FAO category with highest frequency inside a grid box as a representative, one-to-one correspondence two data sets is obtained. This procedure enables the definition of geographical distribution of the coarser-grid ZOBLER values in the finer FAO grid. After mapping, ZOBLER seven texture classes are distributed over the model grid points. Since the parameterization scheme of the Eta/NCEP model requires information on the soil types of Cosby, these soil types are corresponded to the Zobler texture classes, as shown in Table 2. The table also displays β fractions of clay, small silt, large silt, and sand for the considered texture classes, estimated from the clay/sand/silt triangle [*Hillel*, 1982]. Small and large silt classes are considered to have equal fractional contributions [*Tegen and Fung*, 1994].

2.3. Particle Size/Mass Distribution

The total mass of injected dust strongly depends on particle size distribution. In the present model version, four (K=4) particle categories were used, resulting from the structure of desert soils based on content of clay, small silt, large silt, and sand. For each size category k, typical radius (R_k), density (ρ_k), and the ratio between the mass available for uplift and the total mass (γ_k) are estimated [*Tegen and Fung*, 1994], as summarized in Table 3.

The mass of clay particles is estimated to be 1-2 orders of magnitude smaller than particles in the range 1–10 μm. *Tegen and Fung* [1994] assume that a fraction of erodible clay is between 0.02 and 0.17. In our calculations we specify γ_1=0.08.

Radii of silt particles range from 1 to 25 μm. Particles smaller than 10 μm are mainly removed through the wet and turbulent dry deposition processes. Particles larger than 10 μm are basically removed by gravitational settling. In order to take into account such dependence of removal processes on particle size, silt is divided into small (1–10 μm) and large (10–25 μm) fractions. We assume that small and large silt classes contribute with the same amount to wind erosion; that is, γ_2=γ_3=1.

Having atmospheric lifetime of about 1 hour only, sand particles cannot participate in the longer-term atmospheric transport. However, modeling of sand transport may give important information on areas affected by mobile sand dunes. We assume γ_4=0.12 for the sand fraction to be available for erosion.

2.4. Calculation of $(\partial C_k/\partial t)_{SOURCE}$ Term

2.4.1. Surface concentration. The movement of dust particles is mainly caused by saltation (bombardment) process [*Alfaro*, 1997], where the larger particles with diameters greater than 10 μm break soil cohesion forces and release finer particles into the atmosphere. For the wind erosion process, surface features of the atmosphere and soil conditions play a key role in regulating the amount of released dust. The quantity of mobilized dust directly depends on momentum transfer from the atmosphere. On the other hand, soil conditions (soil structure, soil wetness, vegetation cover) dictate if and how much dust will finally be injected into the atmosphere.

In modeling simulations, either surface flux or surface concentration can be used as a lower boundary condition. The "flux" approach is applied in most of the dust models [e.g., *Westphal et al.*, 1987; *Marticorena and Bergametti*, 1995; *Tegen and Fung*, 1994]. In DREAM the concentration as a surface condition is used. In this way, consistency with the Eta/NCEP model approach is kept for the calculation of moisture and heat flux (schemes that use surface parameters as a lower boundary condition).

The released surface concentration of mobilized particles and the corresponding surface vertical flux depends on two groups of parameters: One relates to the structure and state of the soil. The second group describes the turbulent state of the surface atmosphere.

There is no full agreement among different authors about the flux dependence on friction velocity. For example, *Gillette and Passi* [1988] consider the vertical dust flux F_s to be a function of friction velocity, which asymptotically approaches the fourth power of friction velocity:

Table 3. Features of Typical Dust Particles

k	Type	Typical Particle Radius R_k (μm)	Particle Density ρ_{pk} (g cm^{-3})	γ_k
1	clay	0 73	2 50	0 08
2	silt, small	6 10	2.65	1 00
3	silt, large	18 00	2 65	1.00
4	sand	38.00	2.65	0.12

Table 4. Correspondence Between Soil Texture Classes and w'

1	Cosby Soil Types	w' (%)
1	loamy sand	2 5
2	silty clay loam	6.8
3	clay	11.5
4	sandy loam	2.5
5	sandy clay	10 0
6	clay loam	6.8
7	sandy clay loam	3.5

$$F_S = \text{const} \times u_*^4 \left(1 - \frac{u_{*t}}{u_*}\right) \quad \text{for} \quad u_* \geq u_{*t} \tag{5}$$

Here u_* is the friction velocity, and u_{*t} is its threshold value bellow which dust production ceases.

Tegen and Fung [1994] used another functional form for vertical flux:

$$F_S = \text{const} \times u_*^2 (u_* - u_{*t}) \quad \text{for} \quad u_* \geq u_{*t} \tag{6}$$

The study of *Shao et al.* [1993], based on wind tunnel experiments, suggests relationships different than (5) and (6). Their study proposes the following parametric formula for dust surface fluxes:

$$F_S = \text{const} \times u_*^3 \left[1 - \left(\frac{u_{*t}}{u_*}\right)^2\right] \quad \text{for} \quad u_* \geq u_{*t} \tag{7}$$

which is in good agreement with the wind tunnel measurements. This is the relation used as a starting point to develop the new dust production scheme used in this work. Effects of the soil structure and particle size distribution previously described as parameters α, β, and γ (equation (4) and Tables 2 and 3, respectively) are also taken into account. The dust productivity factor is defined as:

$$\delta_k = \alpha \gamma_k \beta_k . \tag{8}$$

Here the subscript k denotes particle size categories. The influence of soil textures is included in β. The effective surface vertical flux can be defined as:

$$F_{Sk}^{\text{EFF}} = \delta_k F_S . \tag{9}$$

The surface concentration can be expressed in terms of vertical surface flux [*Nickling and Gillies*, 1989] in the following form:

$$C_{Sk} = \text{const} \times \frac{F_{Sk}^{\text{EFF}}}{\kappa u_*} . \tag{10}$$

The expression has been evaluated assuming neutral stability conditions, which is an assumption used in most of the field and wind tunnel measurements. However, this limitation is at least partly removed when (10) is applied as the lower boundary condition for the surface viscous/turbulent mixing schemes in the later considerations. These schemes fully take into the account stability and other relevant features of the surface atmosphere.

Combining (7)-(10), the surface concentration can be calculated as

$$C_{Sk} = c_1 \times \delta_k u_*^2 \left[1 - \left(\frac{u_{*tk}}{u_*}\right)^2\right] \quad \text{for} \quad u_* \geq u_{*tk} . \tag{11}$$

The value of the dimensional empirical constant c_1=2.4×10^{-4} m^{-5} kg s^{-2} is determined a posteriori through the model experiments. The dependency of the threshold velocity on particle sizes is elaborated in the following section.

2.4.2. Threshold friction velocity. The threshold friction velocity, at which the soil erosion starts, strongly depends on soil wetness and particle size. Soil water increases the threshold friction velocity, therefore reducing the amount of dust injected into the atmosphere. The water resists in the soil due to capillary forces on surfaces of the soil grains and due to molecular adsorption. In DREAM the soil moisture effects on u_{*t} are included, following the method of *Fecan et al.* [1999]. The maximum amount of the adsorbed water w' is an increasing function of the clay fraction in the soil. On the basis of empirical data, *Fecan et al.* [1999] proposed the calculation of w' as a function of clay content in soil:

$$w' = 0.0014(\%\text{clay})^2 + 0.17(\%\text{clay}) . \tag{12}$$

Combining (12) and β_k from Table 2, the correspondence between w' and the seven considered texture classes is defined (see Table 4). Following available experimental data, *Fecan et al.* [1999] define the threshold velocity in (11) as

$$u_{*tk} = \begin{cases} U_{*tk} & \text{for } w \leq w' \text{ (dry soil)} \\ U_{*tk}\sqrt{1 + 1.21(w - w')^{0.68}} & \text{for } w > w' \text{ (wet soil)} \end{cases} \tag{13}$$

Here w is the ground wetness predicted by the atmospheric model. Following *Bagnold* [1941], the dependency of the threshold friction velocity of dry soil on particle sizes is defined as

$$U_{*tk} = A_k \sqrt{2 g R_k \frac{\rho_{pk} - \rho_a}{\rho_a}} . \tag{14}$$

Here g is gravity acceleration, ρ_{pk} and ρ_a are particle and air densities, respectively. The parameter A_k is only a function of the particle Reynolds number $(Rr)_{pk}=(2R_k U_{*tk})/\nu$ and ν=0.000015 m^2 s^{-1} is the molecular diffusivity for momentum. For the considered four particle sizes in DREAM, A_k={1, 0.7, 0.4, 0.25} is specified by using available empirical data [*White*, 1979].

Although Bagnold-type relation for the threshold friction velocity assumes that there is no flux below U_{*tk}, observations indicate that in case of decreasing u_* the soil erosion does not stop immediately as soon as subthreshold conditions are reached [*Jackson*, 1996]. It is suggested that the particles are carried forward, for a period, due to the inertia and therefore effectively maintaining the transport longer than predicted. In Figure 2 the inertial effect parameterization and the way the underestimation of dust production is avoided is described schematically. The method is functioning as follows: (1) fluxes start to operate when $u_* < u_{*ts}=0.9\times U_{*tk}$ (at time step T_1) increases to the value (at time step T_2); (2) fluxes are still operating when $u_* > U_{*tk}$ (at time step T_2) falls to the value $u_{*st} < u_* < U_{*tk}$ (time steps T_3); (3) fluxes are ceased when $u_{*st} < u_* < U_{*tk}$ (at time steps T_3) stays in the interval $[u_{*st}, U_{*tk}]$ or decrease to $u_* < u_{*st}$ (at time step T_4).

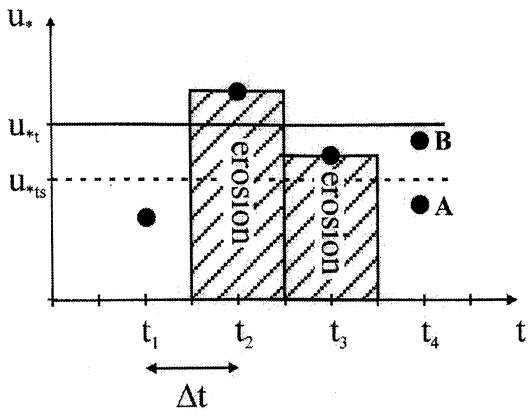

Figure 2. Conceptual model describing dust production under subthreshold friction velocity conditions. At model time step t_1, u_* is below u_{*t}, and there is no dust production. At t_2, u_* exceeds u_{*t} and dust production starts. At t_3, u_* is below the threshold (u_{*t}) but above the subthreshold value (u_{*ts}=0.9u_{*t}), and there is still dust production driven by inertial forces. At t_4, dust production is ceased if either u_* is below u_{*ts} (point A) or even it increases but stays below the threshold (point B).

2.4.3. Viscous sublayer effects. In the Eta/NCEP model, there are two layers operating over the oceans: a thin viscous sublayer located just above the surface having vertical transport realized by molecular diffusion and a layer above with fluxes defined by turbulent mixing [*Janjic*, 1994]. Features of the viscous sublayer are described by different regimes depending on surface turbulent conditions.

Since there is a physical similarity of mass/heat/momentum exchange over surfaces with mobilized particles, such as sea and desert surfaces [*Chamberlain*, 1983; *Segal*, 1990], the same viscous sublayer model was applied for the dust concentration. Following *Janjic* [1994], the dust source term (1) in the concentration equation is represented by

$$\left(\frac{\partial C_k}{\partial t}\right)_{\text{SOURCE}} = -\frac{F_{Sk}}{\Delta z}. \tag{15}$$

Here Δz is the depth of the lowest model layer, k is the subscript denoting the particle size class, and F_{Sk} is the turbulent flux of dust concentration above the viscous sublayer. The turbulent flux can be approximated in terms of the viscous sublayer parameters as

$$F_{Sk} = \nu \frac{C_{0k} - C_{Sk}}{z_C}. \tag{16}$$

The subscript *0* denotes values at the interface of the viscous and turbulent layers, while the subscript *S* denotes the surface values. The depth of the viscous sublayer is approximated by

$$z_C = \frac{0.35 M Rr^{0.25} Sc^{0.5} \nu}{u_*}. \tag{17}$$

Here M is a parameter varying for different turbulent regimes, and u_* is the friction velocity. The roughness Reynolds number Rr and the Schmidt number Sc are defined by

$$Rr = \frac{z_0 u_*}{\nu}, \qquad Sc = \frac{\nu}{\lambda}, \tag{18}$$

λ is the particle diffusivity, and z_0=max(0.018(u_*^2/g), 1.59×10^{-5}) [*Zoumakis and Kelessis*, 1991].

Following *Janjic* [1994], the viscous sublayer for dust transport is assumed to operate in the following regimes: smooth and transitional, rough, and very rough, depending on Rr (or, equivalently, on u_*). Transitions between regimes are assumed to occur at u_{*r}=0.225 m s^{-1} and u_{*s}=0.7 m s^{-1}. Following observational data the parameter M is defined as M=30, for the smooth regime, and M=10 otherwise.

The particle diffusivity λ is many times smaller than ν [*Businger*, 1986]. In the wind-tunnel experiments of *Chamberlain et al.* [1984], synthetic particles with diameter 0.65 μm were used, having diffusivity coefficients λ=4.8×10^{-9} m^2 s^{-1} for smooth and transitional flow, and λ=3.0×10^{-8} m^2 s^{-1} for rough conditions. These values are applied in DREAM. Because of the lack of other measurements, the same values for the four particle sizes were used. For a very rough turbulent regime, λ=7.0×10^{-8} m^2 s^{-1} was adopted.

When the friction velocity exceeds u_{*r}, the smooth regime stops to operate and the flow enters into the rough one. In this case, the viscous sublayer for momentum is turned off, while for the other parameters (including dust) continues to function until the next critical value u_{*s} is achieved. At this point, the rough regime transits to the very rough one by fully developed turbulence. At this stage, the viscous sublayer for dust is completely ceased and extensive mobilization of dust particles starts.

Expression (16) can alternatively be defined in terms of turbulent conditions above the viscous sublayer:

$$F_{Sk} = K_S \frac{C_{LMk} - C_{0k}}{\Delta z}. \tag{19}$$

K_S is the surface-mixing coefficient for concentration, and *LM* denotes the lowest model level. In DREAM, K_S is assumed equivalent to the mixing coefficient for heat and moisture. The surface-mixing coefficient is calculated according to the Monin-Obukhov method [*Janjic*, 1996b].

Requirement that the fluxes (6) and (19) are matched at the interface of the viscous and turbulent layers leads to the lower boundary condition for concentration:

$$C_{0k} = \frac{C_{Sk} + \omega C_{LMk}}{1 + \omega}. \tag{20}$$

$$\omega = \frac{\left(\frac{K_S}{\Delta z}\right)}{\left(\frac{\lambda}{z_C}\right)}, \tag{21}$$

which has a role of weighting factor in (20). From (19) and (20) the surface fluxes are calculated as

$$F_{Sk} = K_S^* \frac{C_{LMk} - C_{Sk}}{\Delta z}. \tag{22}$$

Here C_{Sk} is defined by (11), and

$$K_S^* = \frac{1}{1 + \omega} K_S \tag{23}$$

is a conventional similarity-theory mixing coefficient but corrected by viscous effects.

2.4.4. Shear-free convection effects. Overheated desert surfaces may generate strong uprising thermal plums which

are associated with significant upward vertical transport even in the absence of surface wind shear. In such cases, surface fluxes are calculated differently from (22), following the method of *Zilitinkevich et al.* [1998].

Under the shear-free convection conditions, the friction velocity vanishes causing a singularity in calculation of surface fluxes if a traditional approach (e.g., the Monin-Obukhov theory) is applied. The method of *Beljaars* [1994] applied in the Eta/NCEP model avoids this difficulty by correcting the turbulent kinetic energy with the kinetic energy of the near-surface wind induced by the large-scale eddies [*Janjic*, 1996b], thus preventing the friction velocity and the Obukhov length to get nonzero values. With the Beljaars correction, the surface buoyancy flux $(\overline{w'T'})_S$ is converted into the turbulent kinetic energy of the near-surface wind. The fraction of the surface buoyancy flux converted into the turbulent kinetic energy is assumed to be

$$U_B^2 = (1.2 \times W^*)^2, \tag{24}$$

where the convective scale velocity is defined by

$$W^* = \left[\frac{1}{273} \times gh\left(\overline{w'T'}\right)\right]^{1/3}. \tag{25}$$

Here h is the depth of the convective boundary layer. In practice, the Beljaars correction is performed by adding U_B to the wind speed at the upper boundary of the surface layer.

In practice, at each model time step when the turbulent calculations are made, model points with the shear-free condition fulfilled are distinguished from the others. In such points the vertical flux is calculated following the method of *Zilitinkevich et al.* [1998]. In the remaining points, relation (22) is applied.

The shear-free flow is characterized by strong convection in which buoyancy-driven structures create a narrow uprising motion. Such structures generate a surface convergence, which is superimposed on the mean wind. In the shear-free regime the flow yields its own velocity shear characterized by the "minimum friction velocity" U_* and the "minimum Monin-Obukhov length" L_*. Under these conditions the flow is characterized by a well-developed planetary boundary layer combined with a relatively smooth roughness height. The shear-free convective dust flux is calculated by using the "aerodynamic" mixing coefficient

$$K_{AC} \equiv \frac{F_S}{U_* \Delta C_A}, \tag{26}$$

rather than the bulk coefficient (23) Expression (26) is valid in a broad range of turbulent conditions, for $10^{-10} \le z_{0u}/h \le 10^{-5}$. Here z_{0u} is the roughness length for momentum. The concentration "aerodynamic increment" is formulated by

$$\Delta C_A \equiv C_{AS} - C_{LM} = \left(C_S - \frac{F_C}{\kappa U_*} \ln \frac{z_{0u}}{z_{0C}}\right) - C_{LM}, \tag{27}$$

where κ=0.4 is the von Karman constant, C_{LM} is the lowest model level concentration, C_S is the surface concentration defined by (11), and C_{AS} is the concentration extrapolated logarithmically downward to the level $z=z_{0u}$. Following *Zilitinkevich et al.* [1998], the next approximations are used:

$$\frac{U_*}{W_*} = 0.36\left(\frac{z_{0u}}{h}\right)^{0.1}, \tag{28a}$$

$$K_{AC} = \frac{1}{4.4\left(\frac{h}{z_{0u}}\right)^{0.1} - 1.5}. \tag{28b}$$

These values are in good agreement with available measurements. Finally, by using (26), (27), and (28), the surface flux at shear-free model points is calculated as

$$F_S = \frac{0.36\left(\frac{z_{0u}}{h}\right) W_* (C_S - C_{LM})}{\frac{1}{\kappa} \ln \frac{z_{0u}}{z_{0C}} + 4.4\left(\frac{z_{0u}}{h}\right)^{-1} - 1.7}. \tag{29}$$

2.5. Dust Sinks

2.5.1. Dry deposition. The dry part of particle deposition on the Earth surface is parameterized according to the scheme of *Georgi* [1986]. This scheme includes processes of deposition by surface turbulent diffusion and Brownian diffusion, gravitational settlement, and interception and impaction on the surface roughness elements.

The dry deposition velocity v_{dep} is parameterized by

$$v_{dep} = \frac{1}{\frac{1}{v_{SL}} + \frac{1}{f_{B0} v_{IL}}}. \tag{30}$$

Here v_{SL} is the turbulent deposition velocity in the layer between z_S and 10 m; v_{IL} is the turbulent deposition velocity at the top of the viscous sublayer z_S, and f_{B0} is the empirical constant, which takes into account the effect of the blow-off over the vegetation surfaces. The velocity v_{SL} is expressed as

$$v_{SL} = C_{D10} U_{10} \frac{\sqrt{C_{D10}}}{\sqrt{C_{D0}} - \sqrt{C_{D10}}}, \tag{31}$$

where the drag coefficients $C_{D10} = u_*^2 / U_{10}^2$ and $C_{D0} = u_*^2 / U_{Z_S}^2$ and the velocities U_{10} and U_{Z_S} are specified, with respect to the heights z=10 m and z_S, respectively.

The velocity v_{IL} is parameterized by

$$v_{IL} = G\sqrt{C_{D10}} u_*. \tag{32}$$

The function G, introduced by *Georgi* [1986], reflects the properties of particles (size, composition) and depositing surfaces (roughness, texture, vegetation coverage). It is given by

$$G = \frac{B_{St}}{\sqrt{C_{D0}}}, \tag{33}$$

where B_{St} is the particle surface Stanton number. At the same time, G may be expressed as a sum of contributions from the Brownian diffusion, interception, and impaction [*Slinn*, 1982]:

$$G = G_{BD} + G_{int} + G_{imp}. \tag{34}$$

G is separately considered for two kinds of surfaces: surfaces with turbulent regimes ranging from smooth to rough conditions and surfaces covered by vegetation.

The first kind of surfaces includes sea, bare soil, and ice surfaces. For them, f_{B0}=1 is assumed. Over such surfaces the

Table 5. Values of $C_{D0}^{-0.5}$ and G for Different Turbulent Regimes

Turbulent Regime Defined According to Rr (equation (18))	$C_{D0}^{-0.5}$	G
$Rr<0.13$	13.5	$Sc^{-2/3}+4.27\cdot(St^2/(St^2+400))$
$0.13<Rr<2.00$	$6.432\,Rr^{0.3634}$	$0.6667\cdot Rr^{0.2}\,Sc^{-0.538Rr^{-0.105}}+2.225\cdot Rr^{0.3634}\cdot(St^2/(St^2+400))$
$Rr>2.00$	5	$0.6849\cdot Rr^{0.25}Sc^{0.5}+1.75\,(St^2/(St^2+400))$

parameters $C_{D0}^{-0.5}$ and G are represented by expressions as shown in Table 5. [*Georgi*, 1986] Here $St=(v_g u_*^2)/vg$ is the Stokes number, where the gravitational settling velocity at the lowest model level is defined as

$$(v_{gk}) = \frac{2g\rho_{pk}R_k^2}{9\nu}, \tag{35}$$

where g=9.8 m s^{-1} is the gravitation acceleration, R_k and ρ_{pk} are the radius and density of a kth particle size class, respectively, as given in Table 3.

Equations (30)-(35) and Tables 3 and 5 completely determine the deposition velocity v_{dep}.

For surfaces covered by vegetation, the parameterization proposed by *Georgi* [1986] is used. A number of parameters and constants dependent on vegetation types is defined, as shown in Table 6. Over vegetation surfaces, *Georgi* [1986] defines

$$G = \sqrt{\frac{\eta}{c_{dm}}}, \tag{36}$$

with c_{dm} to be the local drag coefficient for vegetation, depending upon m different vegetation types (see Table 6.) and η the efficiency of vegetation to collect the aerosol. The collection efficiency is approximated by

$$\eta = \eta_{BD} + \eta_{\text{int}} + \eta_{\text{imp}} + \eta_s. \tag{37}$$

The subscripts denote Brownian diffusion, interception, impaction, and collection by small elements, respectively.

The collection efficiency for Brownian diffusion is given by

$$\eta_{BD} = c_{vm}Sc^{-1/3}, \tag{38}$$

where the local viscous drag coefficient c_{vm} depends upon m different vegetation types (see Table 6.).

The collection efficiency for interception depends on particle size k and it is specified as

$$\eta_{\text{int}} = \frac{F_k^2}{\alpha}, \tag{39}$$

where $F_k=R_k/\alpha$, R_k is the radius of the kth particle class, and α=0.5 mm is the average obstacle radius.

The collection efficiency for interception by smaller vegetation elements is defined by

$$\eta_s = A_{sm}F_{sk}\ln(1+F_{sk}), \tag{40}$$

where $F_{sk}=R_k/\alpha_s$, α_s=10 μm. The factor A_{sm} is the ratio between areas of small collectors and area of the roughness elements, which depends upon different vegetation types m (see Table 6).

Finally, the collection efficiency for impaction is approximated by

$$\eta_{\text{imp}} = \frac{St_a^{3/2}}{(St_a+0.6)^{3/2}}, \tag{41}$$

where $St_\alpha=(v_g u_*)/g\alpha$ is the Stanton number over vegetation surfaces.

For particle deposition over surfaces covered by vegetation, $f_{BO}=1/e^{\sqrt{St_\alpha}}$ is used. The parameter $(C_{D0}^{-0.5})_m$ used in the calculations over vegetation surfaces ranges from 2 to 3.5, for different vegetation types m, as is given in Table 6.

In summary, using (38)-(41), (37) can be rewritten as

$$\eta = c_v Sc^{-1/3} + \frac{F^2}{2} + \frac{St_a^{3/2}}{(St_a+0.6)^{3/2}} + A_s F_s \ln(1+F_s). \tag{42}$$

With equations (31)–(42) the dry deposition velocity v_{dep} (30) is fully determined. The contribution of dry deposition to the source term in (1) is then defined as

$$\left(\frac{\partial C}{\partial t}\right)_{\text{SINKddep}} = -\left(\frac{Cv_{dep}}{\Delta z}\right)^{LM}. \tag{43}$$

2.5.2. Wet deposition. In DREAM the wet removal of dust concentration is calculated using the model precipitation water. For each model box, the rate of dust scavenged by precipitation is calculated as

$$\left(\frac{\partial C}{\partial t}\right) = -\phi\frac{\partial}{\partial z}\left(C\frac{\partial P}{\partial t}\right), \tag{44}$$

Table 6. Parameters Related to Deposition Over Surfaces Covered by Vegetation Which Depend on Vegetation Types

M	Vegetation Types According to Dorman/Sellers	c_d	c_v	A_s	$(C_{D0}^{-0.5})_m$
1	broadleaf and evergreen trees	0.50	0.16	0	2.0
2	broadleaf and deciduous trees	0.50	0.16	0	2.0
3	broadleaf and needleleaf trees	0.50	0.16	0	2.0
4	needleleaf and evergreen trees	0.40	0.12	0	2.5
5	needleleaf and deciduous trees	0.40	0.12	0	2.5
6	broadleaf trees with groundcover	0.40	0.12	0	2.5
7	groundcover only or cultivations	0.30	0.08	1.4×10^{-5}	3.5
8	broadleaf shrubs with perennial groundcover	0.35	0.09	3.2×10^{-5}	3.0
9	broadleaf shrubs with groundcover	0.35	0.09	3.2×10^{-5}	3.0
10	dwarf trees and shrubs with groundcover	0.35	0.09	3.2×10^{-5}	3.0

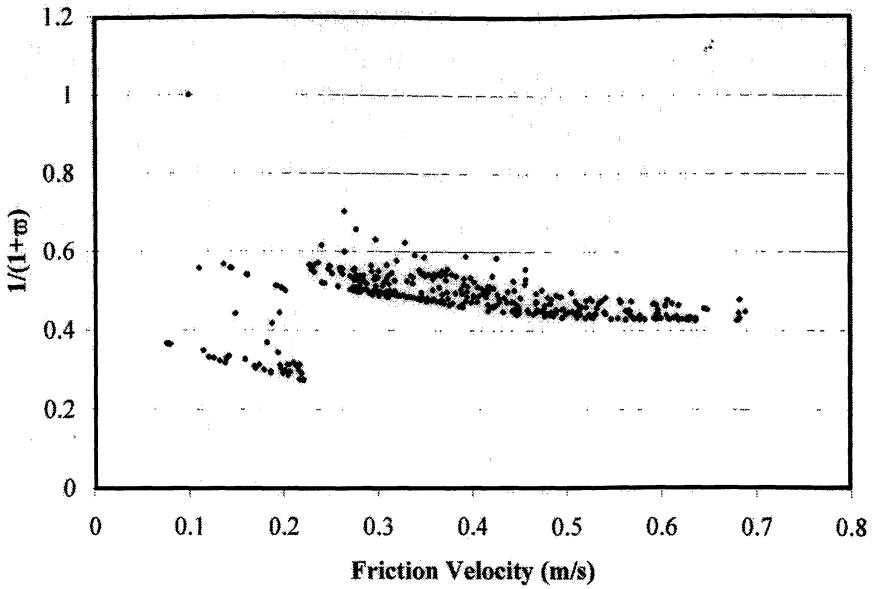

Figure 3. Dust mixing efficiency factor $1/(1+\omega)$ calculated in the model source points as a function of friction velocity.

where $\partial P/\partial t$ is the model precipitation rate, and the constant value of washout parameter $\phi=5\times10^5$ is used. The deposition on the surface is calculated by

$$\left(\frac{\partial C}{\partial t}\right)_{\text{SINKwdep}} = -\phi\left(\frac{C}{\Delta z}\frac{\partial P}{\partial t}\right)^{LM} \tag{45}$$

2.6. Other Model Components Relevant for Concentration Calculations

2.6.1. Horizontal advection. The Eta/NCEP model scheme for advection of a passive substance [*Janjic*, 1997] is conservative, positive definite, and does not create new maxima. The same scheme is used for the horizontal advection of dust concentration, as well. The scheme is the finite-difference approximation of

$$\left(\frac{\partial C}{\partial t}\right)_{\text{hadv}} = -u\frac{\partial C}{\partial x} - v\frac{\partial C}{\partial y}. \tag{46}$$

In this scheme, a first-order upstream advection approximation is used as a first step. As a second step, the advection is followed by the antidiffusion step in which the level of diffusion can be controlled. In one-dimensional form with constant advection speed, the advection is represented by the following approximation:

$$C_j^{n+1} = C_j^n - \mu\frac{C_j^n - C_{j-1}^n}{\Delta x} - \frac{1}{3}\mu\left(C_{j-1}^n - 2C_j^n + C_{j+1}^n\right), \tag{47}$$

where j denotes the grid-point index, n is the time level, $\mu=c(\Delta t/\Delta x)$ is the Courant number, c is the advection speed, and Δx and Δt are the grid size and the time step, respectively.

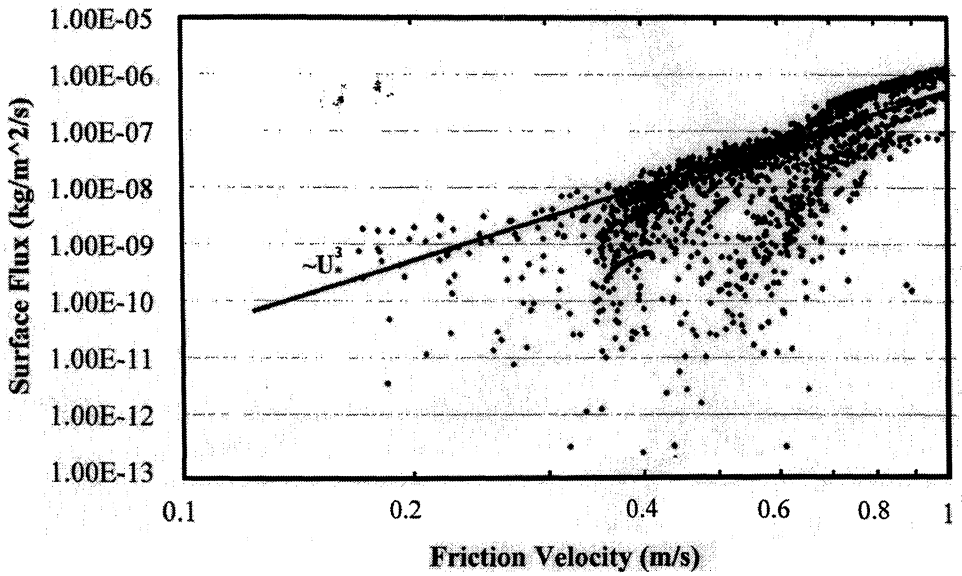

Figure 4. Surface dust flux calculated at the model source points as a function of friction velocity. The solid line is proportional to the third power of friction velocity.

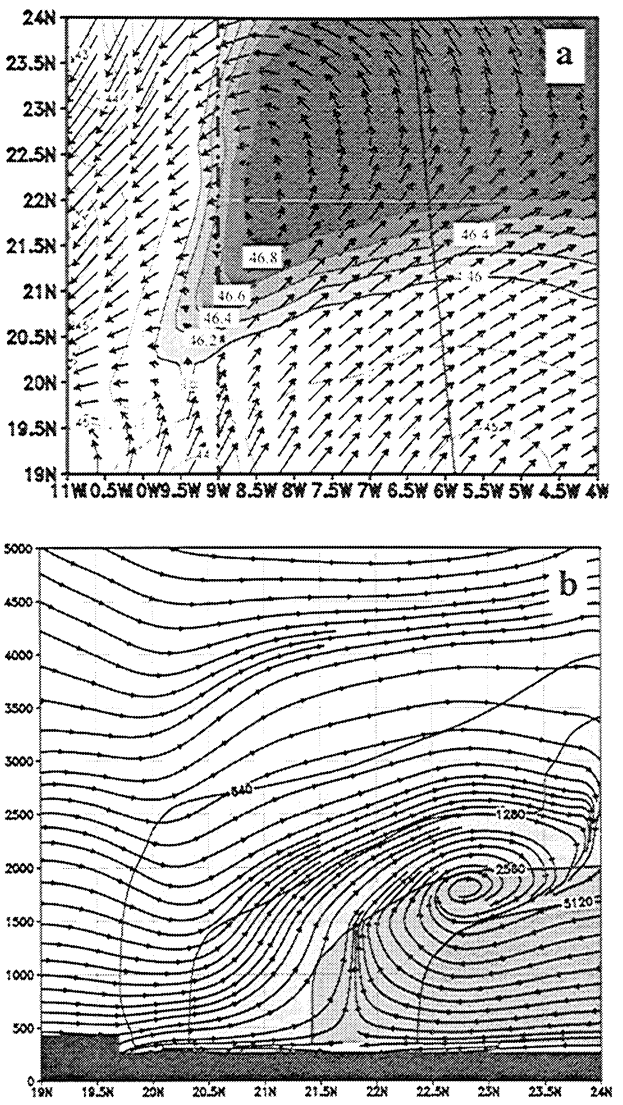

Figure 5. Simulated atmospheric conditions during dust storm over overheated ground in eastern Africa valid on 1800 UTC, June 14, 1993. (top) 10 m wind (arrows) and 2 m temperature (shaded intervals with isolines). (bottom) Vertical section of wind stream function (lines) and concentration (in $\mu g\ m^{-3}$, shaded intervals with isolines), crossing along 9°W. Height (vertical axes) is given in meters

The two-dimensional version of the scheme is obtained as the sum of the contributions along the x and y coordinate axes.

2.6.2. Vertical advection. Conventional advection schemes may produce negative values of positive quantities such as dust concentration. To keep this problem under control, the *Van Leer* [1977] scheme for the vertical advection of concentration is applied. This is the same scheme used for the specific humidity advection, the Eta/NCEP model. The method maintains monotonicity in the calculation of the vertical advection of C. Through a number of readjustment iterations for a given time step, the vertical profile of C is represented by piecewise linear segments. The slope of the C-line segment is never adjusted in layers that contain local extremes. This results in no new minima or maxima created in the vertical profile of C.

Given the values of C on the layer interfaces, the change in C due to the vertical advection is computed according to

$$\left(\frac{\partial C}{\partial t}\right)_{\text{vadv}} = -W\frac{\partial C}{\partial z} = -\frac{\partial}{\partial z}(CW) + C\frac{\partial W}{\partial z}. \quad (48)$$

$W=w-v_g$ is the relative vertical velocity of concentration, where w is the vertical air velocity and v_g is the gravitational settling velocity calculated from the Stokes formula:

$$v_{gk} = \frac{2g\rho_{pk}R_k^2}{9\nu}, \quad (49)$$

with ρ_{pk} to be the particle density, R_k the particle radius, ν the air viscosity, and g the gravitation acceleration.

2.6.3. Vertical diffusion. In the Eta model, a Kolmogorov-Heisenberg turbulence-type closure scheme free of the realizibility problem [*Janjic*, 1990, 1994, 1996b] is applied. An outcome of the turbulent scheme is the vertical mixing coefficients used in the vertical diffusion calculations. In DREAM the vertical diffusion contribution to the concentration variations

$$\left(\frac{\partial C}{\partial t}\right)_{\text{vdiff}} = -\frac{\partial}{\partial z}\left(K_Z\frac{\partial C}{\partial z}\right), \quad (50)$$

is calculated assuming that K_Z is equivalent to the coefficient for temperature and moisture mixing.

2.6.4. Lateral diffusion. In (1) the second-order diffusion scheme

$$\left(\frac{\partial C}{\partial t}\right)_{\text{ldiff}} = -\nabla(K_Z\nabla C), \quad (51)$$

is used by utilizing the Smagorinsky-type horizontal diffusion coefficient modified by the presence of the model turbulent kinetic energy (*TKE*) term [*Janjic*, 1990]:

$$K_H = Fd_{\min}\sqrt{2(\Delta_x u - \Delta_y v)^2 + 2(\Delta_x u + \Delta_y v)^2 + F'TKE}. \quad (52)$$

Here F and F' are empirical constants, $d_{\min}$ is the minimum grid distance, and the operator Δ followed by a subscript denotes the difference between two neighboring values along the coordinate axis indicated by the subscript. The prognostic model parameter *TKE* is included in order to take into the account the effects of horizontal mixing due to dry convective entrainment and detrainment.

3. Review of Major Model Results

Different DREAM components were tested and some compared with available observations. All model simulations were based on real-time meteorological data. The atmospheric part of DREAM was set up using 32 model layers extending from the Earth surface to 100 hPa in the vertical. In the horizontal, different horizontal model resolutions were used, ranging from 0.1° to 1.0° latitude/longitude, depending on experiments. The objective analyses of meteorological parameters from the global model of European Centre for Medium-Range Weather Forecasts were used to define initial and lateral boundary conditions in all the experiments except one, using operational dust forecasts based on NCEP objective analyses. The lateral boundary conditions were

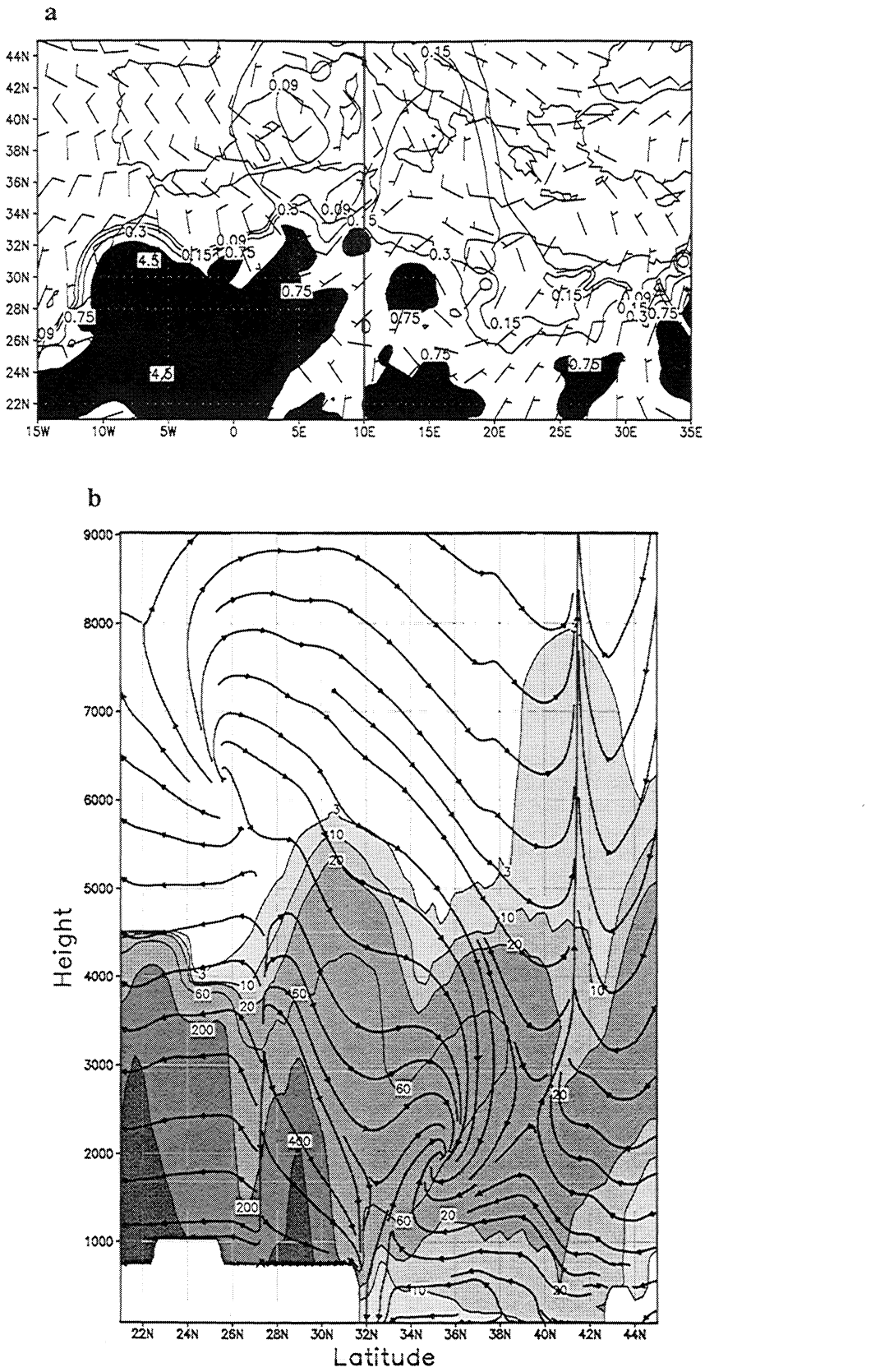

Figure 6. (a) Predicted fields of dust load (units: g m^{-2}, shaded) and 850 hPa wind (barbs), valid for 1200 UTC, July 12, 2000. The line at 10°E indicates the position of the cross section; (b) wind flow (streamlines calculated using meridional/vertical velocities) and dust concentration (shaded, in μg m^{-3}) in the vertical plane crossing 10°E.

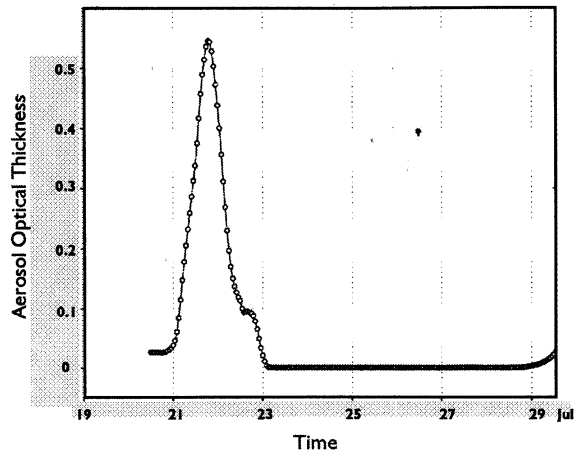

Figure 7. Time evolution of the model aerosol optical thickness collected hourly during the period July 20-30, 2000, at El Arenosillo, southern Spain (31.70°N, 6.10°W).

updated every 6 hours. DREAM was executed in a sequence of coupled 1 day runs by reinitializing the atmospheric fields every 24 hours. The simulated dust concentration of the previous day was used as an update for the next-day model run. The model at the starting day was run using "cold start" conditions, i.e., the zero-concentration initial state. According to our experience, the model needs about 2-3 days for spinning up and for establishing reliable dust concentration conditions.

The aerosol production phase represents a critical point in dust modeling, since larger deviations from real conditions during the major dust storms may lead to poor simulation results of the remaining components of the atmospheric dust cycle. The viscous layer model (equations (22) and (23)) is an important parameterization component regulating the dust production mechanism in the model. The factor $1/(1+\omega)$ appearing in (23) multiplies the conventional surface turbulent coefficient and indicates how much the dust mixing is (effectively) less than the heat/moisture mixing. Figure 3 displays values of this factor calculated in all model source points over a 24 hour simulation. Most of the points fall into the interval 0.4-0.6 for friction velocities higher than 0.225 m s^{-1} (the value at which viscous mixing is ceased). In this range, there is a slight decrease of the factor with respect to the friction velocity.

Additional insight into the behavior of the dust production scheme is obtained by analyzing surface dust fluxes. All fluxes calculated in the model source points over a 24 hour simulation are plotted against the friction velocity in Figure 4. There is a large scattering of fluxes for friction velocities less then 0.3 m s^{-1}. This effect is related to weak turbulent conditions and inertial effects described before. The grouping of points can be noticed at higher friction velocities and the pattern is approximately proportional to the third power of u_*, as parameterized by *Shao et al.* [1993]. *Nickling and Gilles* [1993] also observe similar values. Figure 4 shows existence of a jump in flux values at u_*=0.7 m s^{-1} happening due to entrance of atmospheric flow into a fully developed turbulence regime (see section 2.4.2).

A thermodynamic mechanism related to the shear-free convection may enhance dust lifting during dust storms. To analyze such atmospheric conditions, the model with high horizontal resolution of 0.1° was run over the area covering

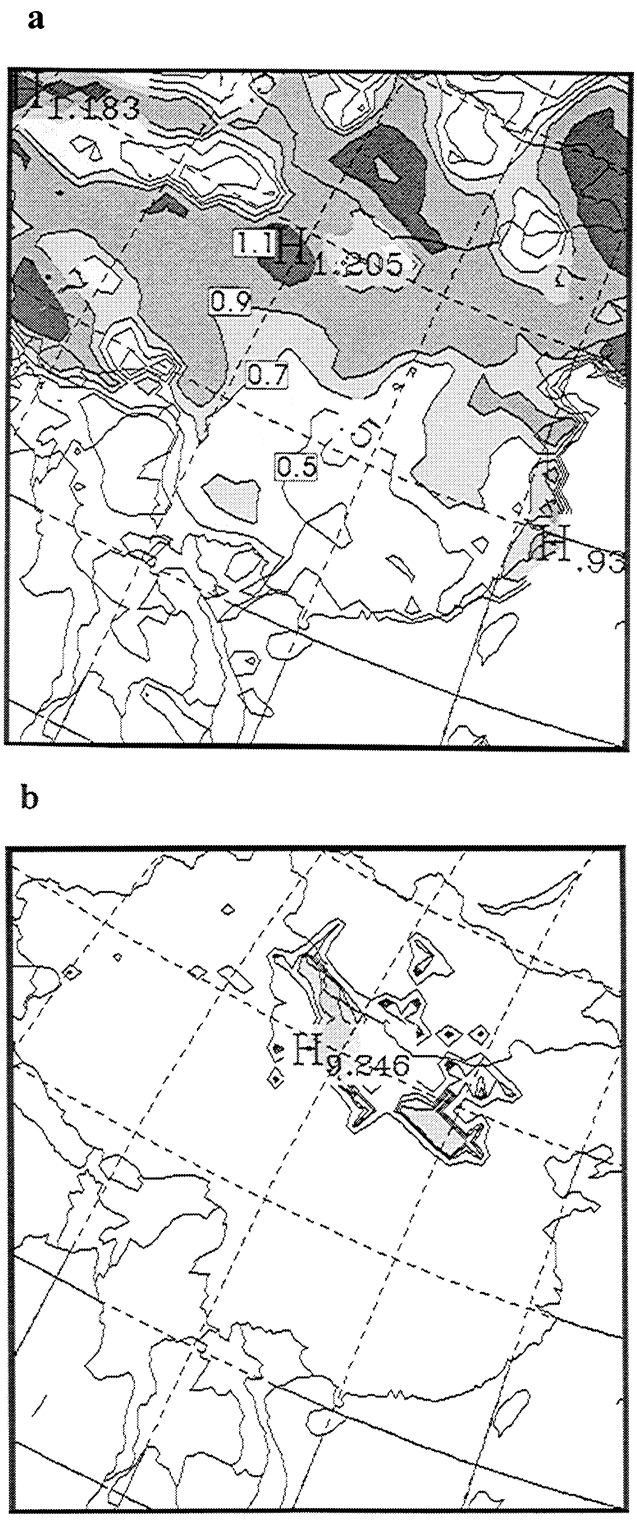

Figure 8. Simulated surface conditions over eastern Asia on April 19, 1998. (a) Friction velocity (in m s^{-1}) and (b) surface dust fluxes (in relative units; for example, value 8 corresponds to 10^{-7} kg m^{-2} s^{-1}, value 9 to 10^{-6} kg m^{-2} s^{-1}, etc.).

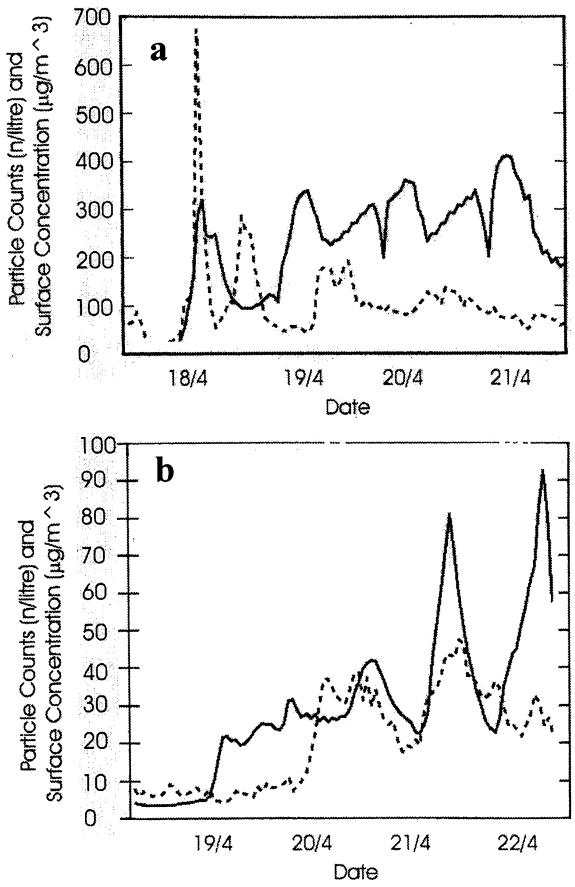

Figure 9. Time evolution of the observed surface concentration (in particle counts/lit, dashed line) and simulated concentration (µg m^{-3}, solid line) (a) in Nagasaki and (b) in Tokyo

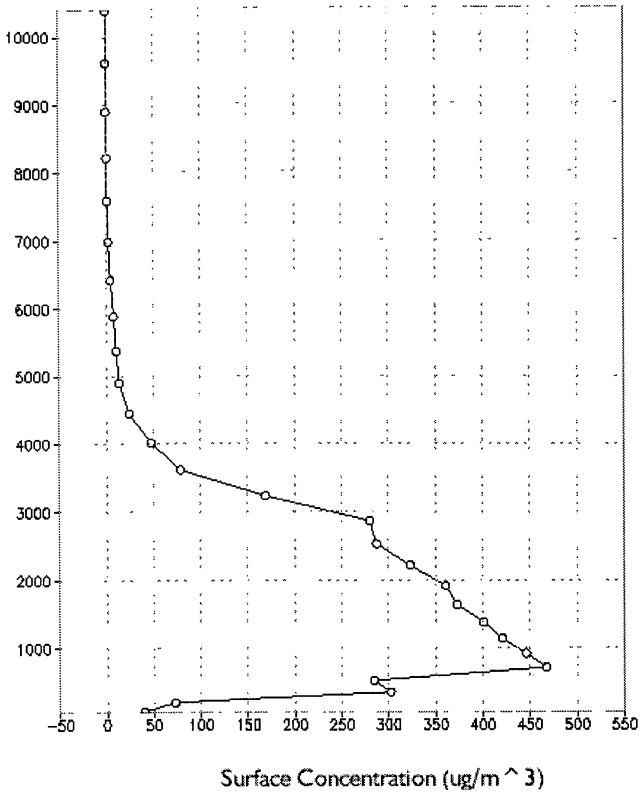

Figure 10. Simulated vertical concentration profile in Okayama on April 20, 1998.

Mauritania and Mali in eastern Africa during June 1993. During this period a large amount of dust was injected into the atmosphere over the considered and surrounding areas, and later transported toward both the Mediterranean and the Atlantic [*Nickovic et al.*, 1997b; *Perry et al.*, 1997]. On June 14, 1800 UTC, the model predicted 2 m temperatures achieving values more than 46°C, and generating local cyclonic surface circulation (Figure 5(top)). The territory around 9°W, 21.5°N was characterized by rather calm flow conditions and high temperatures, which suggested eventual existence of a shear-free convection. Indeed, in the vertical section, crossing along 9°W, one may observe a convergent flow in the lower atmosphere. At the same time, a well-organized upward motion was combined with a secondary curl located at about 1700 m, transporting dust in the vertical (Figure 5(bottom)). The shape of predicted flow is similar to that resulting from the shear-free convection model of *Zilitinkevich et al.* [1998].

Dust may reach the upper troposphere if driven by strong vertical motions. To analyze how the model mechanisms behave under such conditions, a synoptic case of cyclonic system associated with dust load was selected. On July 12, 2000, the 850 hPa wind map shows the existence of a well-organized cyclone in the western Mediterranean (Figure 6a). The cyclone was developed 2 days before and then moved eastward. During this period, favorable surface conditions over western Sahara provided dust storm generation. This process was followed by long-range transport of the lifted dust toward the Mediterranean and

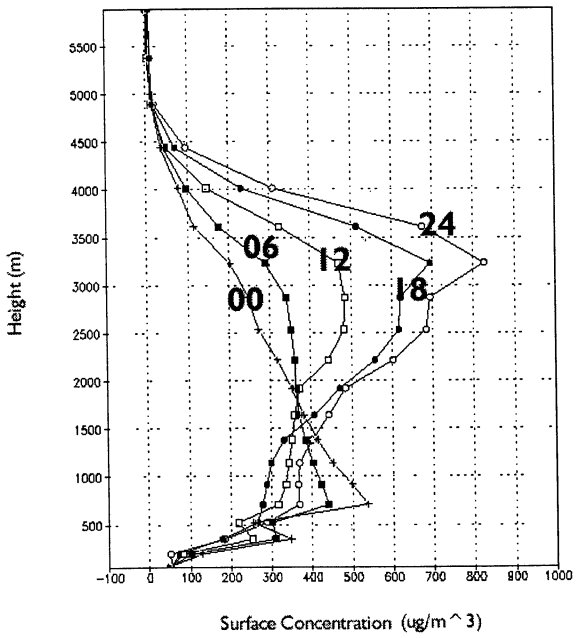

Figure 11. Time evolution of the simulated vertical concentration profile in Nagoya during April 20, 1998.

southern Europe The model was run with 0.3° horizontal resolution. The model simulation indicates existence of substantial dust amount moved away from the sources (Figure 6a). Figure 6b shows the simulated wind flow and concentration distribution in the vertical cross section valid for July 12. The cross-section plane was located at 10°E, passing thus the eastern sector of the cyclone in which the model predicts precipitation as well (not shown). The figure shows existence of well-organized deep-convection structure placed at about 42° Because of a strong upward motion, dust was lifted up to about 8 km.

To check the overall model performance, two additional cases were analyzed for which certain observational evidence exists. The first case is related to the operational DREAM dust forecasts over the Mediterranean (http://www.icod.org.mt/Modelling/HydDyn_main.htm) This simulation is with horizontal grid increment of 0 3° Aerosol optical thickness were calculated (at 1 hour interval) during the period July 20-30, 2000, at El Arenosillo, southern Spain (31 70°N, 6.10°W), where the AERONET (AErosol RObotic NETwork) Sun photometer station is operating as well. During the considered period, a major dust storm was generated on July 20 in the western Sahara, causing passage of dust load over El Arenosillo on July 21. Until the end of the period the model did not predict any new dust activity over Spain. The predicted aerosol optical thickness at El Arenosillo on July 21 compares reasonably well with the El Arenosillo observations (http://www.aeronet.gsfc.nasa.gov), in terms of both (1) time of occurrence and (2) values of increased concentration (Figure 7). Namely, the predicted aerosol optical thickness reaches the maximum of 0.55 about 3 hours later than the observed thickness ranging from 0 3 to 0.5.

Additional simulations were made for the spectacular Asian dust storm of April 1998 [*Husar et al.*, this issue]. The model was run from April 13 to 27 over an area covering eastern Asia, northern Pacific, and the Californian coast. The model simulated exceptionally high dust activity with picks on April 15/16 and 19. The event was triggered by a deep cyclone generated over the northern central China and southern Mongolia. On April 19 the model predicted patterns with high friction velocities, reaching a maximum of 1.2 m s^{-1} (it corresponds to about 30 m s^{-1} of the 10 m wind speed) (Figure 8a). The associated intense surface turbulence was generating surface dust fluxes exceeding 10^{-5} kg m^{-2} s^{-1} (Figure 8b). Such high fluxes are reaching limits that are observed only during huge dust events [*Nickling and Gilles*, 1993; *Marticorena et al.*, 1997]. After injecting into the atmosphere, the dust was driven by the upper airflow pattern toward the Pacific Ocean. This had as a result increased surface concentrations in Nagasaki on April 18, 1998 [*Arao et al.*, 1999; *Murayama et al.*, 1998]. The simulated time of dust arrival corresponds to the observed time (Figure 9a). Until

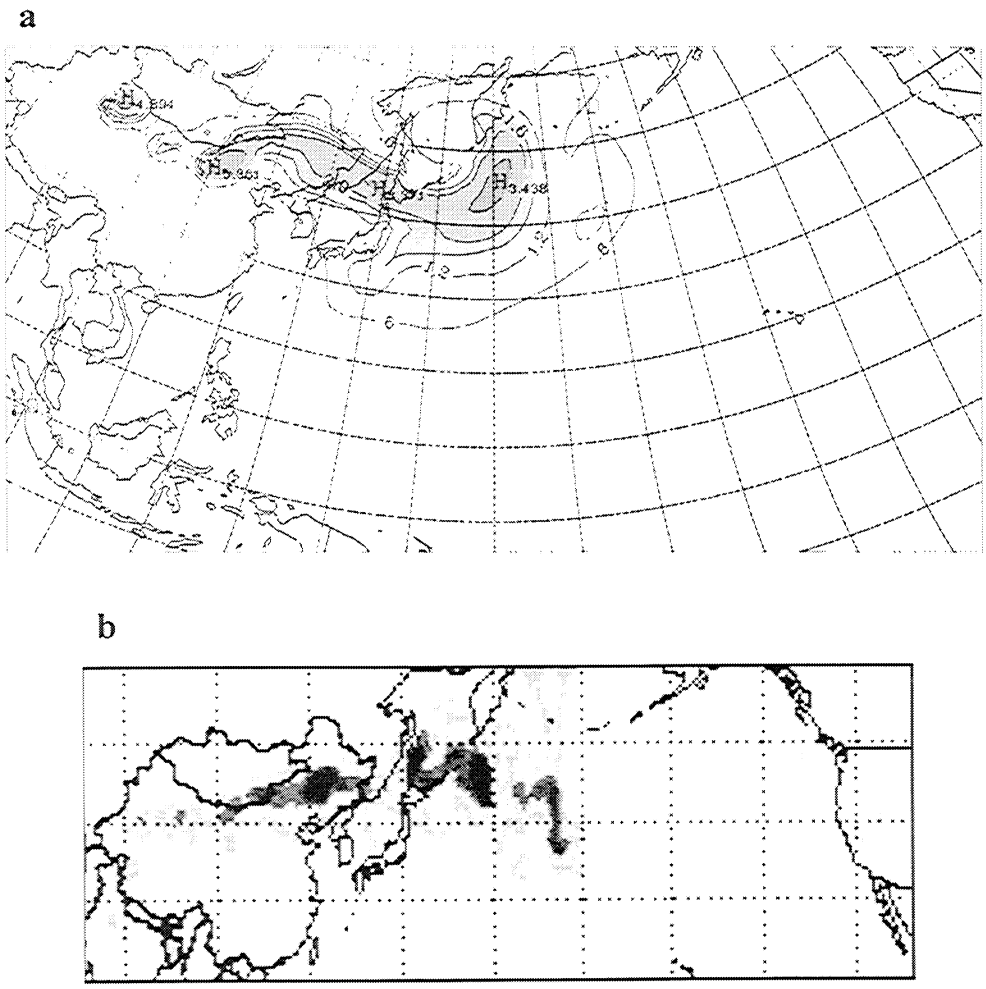

Figure 12. Transport of dust over Pacific during April 21, 1998. (a) Simulated dust load (in g m^{-2}) and (b) aerosol index calculated from data of TOMS satellite.

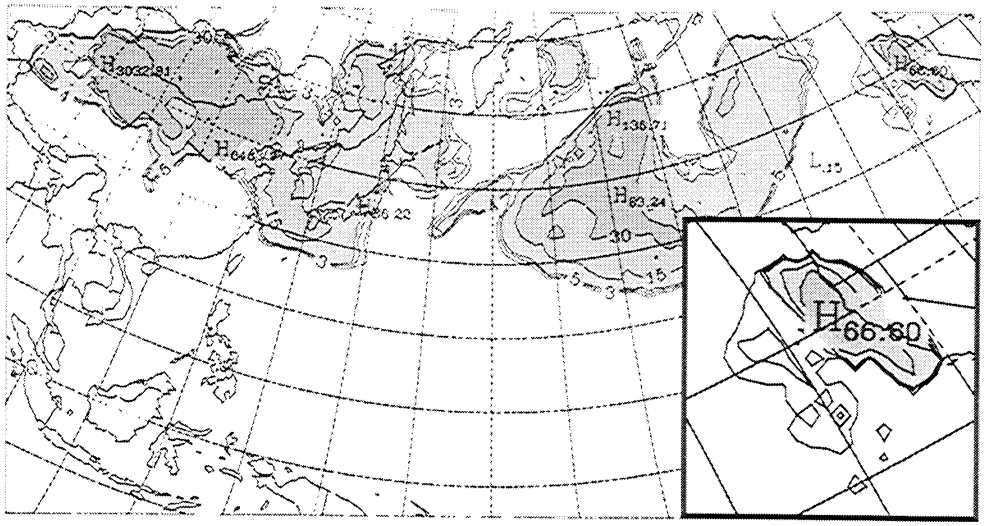

Figure 13. Surface concentration (in μg m^{-3}) over the coast of California (top right-hand corner) on April 26, 1998.

April 21, the model overestimates dust activity over Nagasaki compared to the available observations. In Tokyo the dust arrived 2 days later with smaller concentrations compared to these in Nagasaki, as the observations indicate. Figure 9b shows that the model concentration increases about 1 day earlier compared to the measurements.

Over Japan the model predicts existence of a relatively shallow and low-level dust layer. In Okayama the simulated concentration on April 20 has a maximum at about 1 km (Figure 10), as indicated also by the polarization lidar observations [*Murayama et al.*, 1998]. Figure 11 shows the time evolution of the simulated vertical concentration profile in Nagoya on April 20. The predicted concentration maximum is located at about 3 km, which is in good agreement with the lidar measurements [*Murayama et al.*, this issue].

On April 21, the model predicted a well-developed medusa-like structure of dust load, extending from eastern Asia to 180° meridian in the north Pacific (Figure 12a). The simulated dust-load field is compared with the aerosol index (AI), the parameter that describes the level of UV absorption [*Herman et al.*, 1996]. Despite the fact that there is no straightforward way to convert dust load to AI, the position and shapes of the two fields show a general similarity (Figure 12b). A few days later, a first surface concentration was observed at the western coast of United States [see *Husar et al.*, this issue]. The simulated time and values of surface concentrations coincide with observations (Figure 13)

4. Conclusions

To simulate and/or operationally predict the atmospheric dust cycle (uptake-transport-deposition), a model has been developed, parameterizing the relevant processes The sophisticated SKIRON/Eta modeling system was selected with its "heart" the Eta/NCEP regional atmospheric model in order to drive the embedded dust concentration equation The dust mass is described by particles with four sizes. A dust production scheme is designed taking into account different effects, such as viscous/turbulent mixing, shear-free convection diffusion, and soil moisture. The model parameterizes both wet and dry deposition, the later being dependent on particle size structure and type of collecting surfaces. Different model components have been tested and compared with available observations. In general, the model has demonstrated ability to reproduce major features of the atmospheric dust cycle in a satisfactory way.

Acknowledgments. This research was supported by several research projects: Project MEDUSE (contract ENV4-CT95-0036) funded by the DG-XII of EU; Project SKIRON (contract EPET-II 322) funded jointly by the General Secretariat of Science and Technology of Greece and EU; and Project COMPASS funded by the 4th Italian-Maltese Financial Protocol. Authors thank T Murayama, (University of Mercantile Marine), K. Arao (Nagasaki University), and M Abo (Tokyo Metropolitan University) for providing measurements over Japan Figure 12b is based on TOMS NASA products available on http://jwocky gsfc nasa.gov/aerosols. Authors are also grateful to D Nickovic and G Pejanovic (Euro-Mediterranean Centre for Insular Coastal Dynamics, Malta) for preparing figures Finally, we would like to thank the anonymous reviewers for their constructive comments

References

Alfaro, S C , A Gaudichet, L Gomes, and M Maille, Modeling the size distribution of a soil aerosol produced by sandblasting, *J Geophys. Res , 102,* 11,239-11,249, 1997

Andreae, M O , Raising dust in the greenhouse, *Nature, 380,* 389-340,1996

Arakawa, A , Computational design for long-term numerical integration of the equations of fluid motion: Two dimensional incompressible flow, part I, *J Comp Phys., 1,* 119-143, 1966

Arao, K , and C Sakaguchi, Yellow sand events measured by an optical particle counter at Nagasaki University in 1996-1998 (in Japanese), *J Environ Stud., 1,* 175-186, 1999.

Bagnold, R A , *The Physics of Blown Sand and Desert Dunes,* 265 pp., Morrow, New York, 1941

Beljaars, A. C M , The parameterization of surface fluxes in large-scale models under free convection, *Q J R. Meteorol Soc , 121,* 255-270, 1994

Betts, A , A new convective adjustment scheme, part I, Observational and theoretical basis, *J Meteorol Soc , 112,* 677-693, 1986

Businger, J A , Evaluation of the accuracy with which dry deposition can be measured with current micrometeorologic techniques, *J Clim. Appl Meteorol , 25,* 1100-1124, 1986.

Chamberlain, A C , Roughness length of sea, sand and snow, *Boundary Layer Meteorol., 25,* 405-409, 1983.

Chamberlain, A. C., J A. Garland, and A. C. Wells, Transport of gasses and particles to surfaces with widely spaced roughness elements, *Boundary Layer Meteorol , 24,* 343-360, 1984.

Chen F., K. Mitchell, Z. Janjic, and M. Baldwin, Land-surface parameterization in the NCEP Mesoscale Eta Model, in *Research Activities in Atmospheric and Oceanic Modelling,* World Meteorol. Organ., Geneva, Switzerland, 1996.

Corine, I , Land cover–Technical guide, *EUR 12585 EN,* Comm of the Eur. Commun., Luxemburg, 1993

Dulac, F., D. Tanre, G Bergametti, P. Buat-Menard, M. Desbois, and D Sutton, Assessment of the African airborne dust mass over the western Mediterranean Sea using Meteosat data, *J Geophys. Res., 97,* 2489-2506, 1992

Dulac, F., C. Moulin, C. E. Lambert, F Guillard, J Poitou, W. Guelle, C. R. Quetel, X. Schneider, and U Ezat, Quantitative remote sensing of African dust transport to the Mediterranean, in *The Impact of Desert Dust Across the Mediterranean,* edited by S. Guerzoni and R Chester, pp 25-49, Kluwer Acad., Norwell, Mass , 1996

Environmental Protection Agency (EPA), Global Ecosystem Database, Version 1.0 (on CD ROM) *Documentation Manual,* EPA Global Change Research Program–NOAA/NGDC Global Change Database Program, USDC, Boulder, Colorado, 1992

Fecan, F , B. Marticorena, and G Bergametti, Parameterization of the increase of the Aeolian erosion threshold wind friction velocity due to soil moisture for arid and semi-arid areas. *Annales Geophys., 17,* 194-157, 1999.

Fels, S. B., and M D. Schwartzkopf, The simplified exchange approximation: A new method for radiative transfer calculations, *J. Atmos. Sci., 32,* 1475-1488, 1975.

Georgi, F , A particle dry-deposition parameterization scheme for use in tracer transport models, *J Geophys. Res., 91,* 9794-9806, 1986

Gillette, D. A., and R. Passi, Modeling dust emission caused by wind erosion, *J Geophys Res., 93,* 14,233-14,242, 1988.

Hedin, L. O., and G E Likens, Atmospheric dust and acid rain, *Sci. Am., 12,* 56-60, 1996

Herman, J. R., P. K. Bhartia, O. Torres, C Hsu, C. Seftor, and E, Celarier, Global distribution of UV-absorbing aerosols from Nimbus-7/TOMS data, *J. Geophys Res., 102,* 16,911-16929, 1996

Hillel, D , *Introduction to Soil Physics*, 364 pp., Academic, San Diego, Calif , 1982

Husar, R B , et al., The Asian dust events of April 1998, *J Geophys. Res.*, this issue.

Jackson, D W. T., Potential inertial effects in Aeolian sand transport: Preliminary results, *Sediment Geol., 106,* 193-201, 1996

Janjic, Z I., Pressure gradient force and advection scheme used for forecasting with steep and small scale topography, *Contrib Atmos Phys , 50,* 186-199, 1977

Janjic, Z I , Forward-backward scheme modified to prevent two-grid-interval noise and its application in sigma coordinate models, *Contrib Atmos Phys., 52,* 69-84, 1979.

Janjic, Z I , Non-linear advection schemes and energy cascade on semi-staggered grids, *Mon Weather Rev , 112,* 1234-1245, 1984

Janjic, Z I , The step-mountain coordinate: Physical package, *Mon Weather Rev , 118,* 1429-1443, 1990

Janjic, Z I , The step-mountain Eta coordinate model: Further developments of the convection, viscous sublayer and turbulence closure schemes, *Mon. Weather Rev , 122,* 927-945, 1994

Janjic Z I , The Mellor-Yamada Level 2 5 turbulence closure scheme in the NCEP Eta model, in *Research Activities in Atmospheric and Oceanic Modeling*, edited by H Ritchie, World Meteorol Organ , Geneva, Switzerland, 1996a

Janjic Z I., The surface layer parameterization in the NCEP Eta model, in *Research Activities in Atmospheric and Oceanic Modeling*, edited by H Ritchie, World Meteorol. Organ., Geneva, Switzerland, 1996b.

Janjic Z I., Advection scheme for passive substance in the NCEP Eta model, in *Research Activities in Atmospheric and Oceanic Modeling*, edited by H Ritchie, World Meteorol. Organ., Switzerland, 1997

Joussaume, S., Three-dimensional simulations of the atmospheric cycle of desert dust particles using a general circulation model, *J Geophys Res., 95,* 1909-1941, 1990

Kallos, G , et al , The Regional Weather Forecasting System SKIRON: An overview, in *Proceedings of the Symposium on Regional Weather Prediction on Parallel Computer Environments,* edited by G Kallos, V. Kotroni, and K. Lagouvardos, pp. 109-122, Univ. of Athens, Greece, 1997

Kremling, K., and P. Streau, Saharan dust influenced trace element fluxes in deep North Atlantic subtropical waters, *Deep Sea Res., I(40),* 1155-1168, 1993.

Krichak, S.O., M. Tsidulko, P. Alpert, A. Papadopoulos, O. Kakaliagou, and G Kallos, Eta Weather prediction system with the aerosol production/transport/deposition at TAU, in *Research Activities in Atmospheric and Oceanic Modeling,* edited by H. Ritchie, 28pp., World Meteorol. Organ., Geneva, Switzerland, 1999

Kubilay, N., S. Nickovic, C. Moulin, and F. Dulac, An illustration of the transport and deposition of mineral dust onto the eastern Mediterranean, *Atmos. Environ , 34,* 1293-1303, 2000.

Lacis, A A , and J. E. Hansen, A parameterization of the absorption of air-solar radiation in the earth's atmosphere, *J. Atmos Sci., 31,* 118-133, 1974.

Li, X , H. Maring, D Savoie, K. Voss, and J. M. Prospero, Dominance of mineral dust in aerosol light scattering in the North Atlantic trade winds, *Nature, 380,* 416-419, 1996

Marticorena, B , and G. Bergametti, Modeling the atmospheric dust cycle, 1, Design of a soil-derived dust emission scheme, *J. Geophys Res , 100,* 16,415-16,430, 1995

Marticorena, B , G Bergametti, B. Aumont, Y. Callot, C. N'Doume, and M Legrand, Modeling the atmospheric dust cycle, 1, Simulation of Saharan dust sources, *J Geophys. Res., 102,* 4387-4404, 1997.

Martin, J K , and S E Fitzawater, Ion deficiency limits phytoplankton growth in the North-East Pacific subarctic, *Nature, 331,* 341-343, 1988

Mesinger, F., Z.I Janjic, S. Nickovic, D Gavrilov, and D G. Deaven, The step-mountain coordinate: Model description and performance for cases of Alpine lee cyclogenesis and for a case of an Appalachian redevelopment, *Mon. Weather Rev., 116,* 1493-1518, 1988.

Moulin, C , C E Lambert, F. Dulac, and U. Dayan, Control of atmospheric export of dust from North Africa by the North Atlantic Oscillation, *Nature, 387,* 691-694, 1997.

Murayama, T , et al , Lidar network observation of Asian dust (Kosa) in Japan, in *Proc. SPIE, 3504,* 8-15, 1998.

Murayama, T , et al., Ground-based network observation of Asian dust events of April 1998 in east Asia, *J Geophys Res* , this issue

Nickling, W G., and J. A. Gillies, Emission of fine-grained particulates from desert soils, in *Paleoclimatology and Paleometeorology: Modern and Past Patterns of Global Atmospheric Transport,* edited by M. Leinen, and M Sarnthein, pp 133-165, Kluwer Acad , Norwell, Mass., 1989.

Nickling, W. G., and J. A Gillies, Dust emission and transport in Mali, West Africa, *Sedimentology, 40,* 859-868, 1993.

Nickovic, S., and S Dobricic, A model for long-range transport of desert dust, *Mon Weather Rev , 124,* 2537-2544, 1996.

Nickovic, S , D Jovic, O Kakaliagou, and G. Kallos, Production and long-range transport of desert dust in the Mediterranean region: Eta model simulations, in *Proceedings of the 22nd NATO/CCMS International Technical Meeting on Air Pollution Modelling and Its Applications,* 2-6 June 1997, Clermont-Ferrand, France, 1997a

Nickovic, S., G Kallos, O Kakaliagou, and D Jovic, Aerosol production/transport/deposition process in the Eta model: Desert dust simulations, in *Proceedings of the Symposium on Regional Weather Prediction on Parallel Computer Environments,* edited by G. Kallos, V Kotroni, and K Lagouvardos, pp. 137-145, Univ of Athens, Greece, 1997b

Papadopoulos, A , G. Kallos, S. Nickovic, D. Jovic, M. Dacic, and P. Katsafados, Sensitivity studies of the surface and radiation parameterization schemes of the SKIRON system, in *Proceedings of the Symposium on Regional Weather Prediction on Parallel Computer Environments,* edited by G. Kallos, V. Kotroni, and K. Lagouvardos, pp 155-164, Univ. of Athens, Greece, 1997

Perry, K D , T.A Cahill, R.A. Eldred, and D D. Dutcher, Long-range transport of North African dust to the eastern Union States, *J Geophys. Res , 102,* 11,225-11,238, 1997.

Reichholf, J H , Is Saharan dust a major source of nutrients for the Amazonian rain forest, *Stud. Neotrop. Fauna Environ.*, 21, 251-255, 1986

Segal, M., On the impact of thermal stability on some rough flow effects over mobile surfaces, *Boundary Layer Meteorol*, *52*, 193-198, 1990.

Shao, Y., M. R. Raupach, and P. A. Findlater, Effect of saltation bombardment on the entrainment of dust by wind, *J. Geophys. Res.*, *98*, 12,719-12,726, 1993.

Slinn, W G N, Prediction for particle deposition to vegetative canopies, *Atmos Environ*, *16*, 1785-1794, 1982.

Tegen, I, and I Fung, Modeling of mineral dust in the atmosphere: Sources, transport, and optical thickness, *J Geophys. Res.*, *99*, 22,987-22,914, 1994.

Van Leer, B, Towards the ultimate conservative difference scheme, IV, A second-order sequel to Godunov's method, *J. Comput. Phys*, *32*, 101-136, 1979

Westphal, D L., O B Toon, and T N Carlson, A two-dimensional numerical investigation of the dynamics and microphysics of Saharan dust storms, *J Geophys. Res*, *92*, 3027-3049, 1987

Westphal, D L., O B Toon, and T N. Carlson, A case study of mobilization and transport of Saharan dust, *J. Atmos. Sci.*, *45*, 2145-2175, 1988

White, B. R., Soil transport by winds in Mars, *J. Geophys. Res.*, *84*, 4643-4651, 1979

Wilson, M F, and A Henderson-Sellers, Land cover and soils data sets for use in general circulation climate models, *J. Climatol*, *5*, 119-143, 1985

Zhao, Q, and F H. Carr, A prognostic cloud scheme for operational NWP models, *Mon. Weather Rev*, *125*, 1931–1953, 1997

Zilitinkevich, S S, Non-local turbulent transport: Pollution dispersion aspects of coherent structure of convective flows, in *Air Pollution, III, vol I, Air Pollution Theory and Simulation*, edited by H. Power, N. Moussiopoulos, and C A Brebbia, pp. 53-60, Comput. Mech Publ., Southampton Boston, Mass., 1995.

Zilitinkevich, S, A A. Grachev, and J. C. R. Hunt, Surface frictional processes and non-local heat/mass transfer in the shear-free convective boundary layer, in *Buoyant Convection in Geophysical Flows*, edited by E. J Plate et al., pp. 83-113, Kluwer Acad Norwell, Mass, 1998

Zoumakis, N. M, and A. G Kelessis, The dependence of the bulk Richardson number on stability in the surface layer, *Boundary Layer Meteorol*, *57*, 407-414, 1991

O Kakaliagou, G Kallos, and A Papadopoulos, University of Athens, Department of Applied Physics, Panepistimioupolis Bldg., Phys-V, Athens 15784, Greece (kallos@mg uoa gr)

S Nickovic, Euro-Mediterranean Centre on Insular Coastal Dynamics (ICoD), University of Malta, Foundation for International Studies, St Paul Street, Valletta, Malta (nicko@icod.org.mt)

(Received January 11, 2000; revised November 27, 2000; accepted December 1, 2000)